Designing Production-Optimal Alternative Fuels for Conventional, Flexible-Fuel, and Ultra-High Efficiency Engines

Andrea König[a], Maximilian Siska[a], Artur M. Schweidtmann[a], Jan G. Rittig[a], Jörn Viell[a], Alexander Mitsos[c,a,b], Manuel Dahmen[b,*]

[a] *Process Systems Engineering (AVT.SVT), RWTH Aachen University, 52074 Aachen, Germany*
[b] *Forschungszentrum Jülich GmbH, Institute for Energy and Climate Research IEK-10: Energy Systems Engineering, 52425 Jülich, Germany*
[c] *JARA-ENERGY, 52056 Aachen, Germany*

Abstract

Road transportation needs to abandon fossil fuels. One promising alternative are renewable fuels for internal combustion engines. We consider three competing types of spark-ignition engines, i.e., conventional spark-ignition engines (CSIEs), flexible fuel vehicle engines (FFVEs), and ultra-high efficiency engines (UHEEs), which all have different fuel requirements. To determine which engine-fuel combination is optimal regarding fuel production cost and global warming impact (GWI), we apply our integrated fuel and process design method [König, et al. 2020. Comput. Chem. Eng.]. Specifically, we consider 47 pre-screened fuel species, their selective production routes from renewable resources, and a surrogate for optional blending of fossil gasoline. The designed FFVE (UHEE) fuels reduce GWI by up to 87% (84%) compared to fossil gasoline. In contrast, optimal CSIE fuels only achieve up to 60% GWI reduction and only at higher cost. The superior production performance of selectively-produced UHEE and FFVE fuels motivates replacement of today's CSIE technology.

Keywords: integrated product and process design; fuel design; Process Network Flux Analysis; advanced engine concepts; flexible fuel vehicles; spark-ignition

*Corresponding Author: Manuel Dahmen
Email address: m.dahmen@fz-juelich.de (Manuel Dahmen)

1. Introduction

Road transportation accounts for almost 75% of CO_2 emissions of the global transport sector (Teter et al., 2019). These emissions are largely caused by combusting fossil fuels in internal combustion engines (ICEs). To mitigate the associated adverse climate effects, alternative fuel and engine concepts are being developed (Boot, 2016; Dahmen & Marquardt, 2016; Hoppe et al., 2015; Leitner et al., 2017; Marquardt et al., 2010; Johnson & Joshi, 2018; Sjöberg, 2017). In this context, a large variety of renewable fuel components and associated production pathways have been proposed, which consider feedstocks like lignocellulosic biomass, H_2 from renewable electricity, and/or CO_2 from carbon capture (Huber et al., 2006; Kohli et al., 2019; König et al., 2019; Leitner et al., 2017; Straathof, 2014; Tremel et al., 2015; Ulonska et al., 2016b). Due to the relatively high oxygen content of lignocellulosic biomass, many selective bio-based production pathways lead to oxygenated species (Huber et al., 2006; Marquardt et al., 2010). These oxygenates significantly differ from fossil gasoline regarding their physico-chemical properties. The feasibility of blending such oxygenates in fuels depends on the engine type and corresponding fuel requirements: Conventional spark-ignition engines (CSIEs) can operate on fuels with low oxygen content only. This results, for instance, in a maximum ethanol limit of 10 vol-% (Energy Information Administration, 2020; DIN Deutsches Institut fuer Normung e.V., 2017), whereas flexible fuel vehicle engines (FFVEs) allow for fuels with up to 85 vol-% ethanol (Ford Motor Company, 2020; DIN Deutsches Institut fuer Normung e.V., 2018). While both CSIEs and FFVEs are already commercially available, ultra-high efficiency engines (UHEEs) and corresponding fuels are still in the research phase (Hoppe et al., 2015; Johnson & Joshi, 2018) and would therefore require substantial investments in technology development before being brought to market. However, fuel production benefits might arise since UHEEs can be tailored to the properties of renewable fuels (Dahmen & Marquardt, 2016;

Hoppe et al., 2015; Larsen et al., 2009; Sjöberg, 2017). Aiming at a cleaner and more efficient combustion, UHEEs demand for extremely knock-resistant fuels (Dahmen & Marquardt, 2017; Hoppe et al., 2015; König et al., 2020b; Prakash et al., 2018; Remmert et al., 2014), which can be achieved with certain renewable fuel components (Boot et al., 2017; McCormick et al., 2017).

Given the three engine concepts, their fuel requirements, and various proposed renewable fuel components and associated production pathways, the question arises which fuel-engine combination exhibits the highest potential with regard to fuel production cost and global warming impact (GWI). To answer this question, we utilize model-based fuel design (König et al., 2020b) to optimize fuels and their production pathways for the three engine types and compare the results to each other.

Model-based fuel design can refer to the computer-aided generation of single fuel molecules (Hada et al., 2014; Dahmen & Marquardt, 2016), the formulation of fuel blends (Hashim et al., 2017; Dahmen & Marquardt, 2017) or a combination of the two, i.e., generation of fuel molecules for optimal blends (Yunus et al., 2014; Zhang et al., 2018). Regarding the formulation of blends, the fuel composition is typically optimized for one or multiple objectives subject to a set of possible pre-defined fuel components, mixing rules for physico-chemical properties, and a set of fuel property requirements that is derived from the technical engine needs (Conte et al., 2011; Yunus et al., 2014). While some studies focus solely on the fuel composition as the degree of freedom (Ariffin Kashinath et al., 2012; Hashim et al., 2017; Kalakul et al., 2018; Yunus et al., 2014), others additionally co-optimize a set of possible fuel production pathways, thus accounting for possible (co-)production benefits of different fuel components (Marvin et al., 2013; Dahmen & Marquardt, 2017; König et al., 2020b). In particular, our recently published integrated design method is capable of co-optimizing fuels and their production processes based on the process emissions, i.e., GWI, and fuel production cost (König et al., 2020b). However, neither König et al. (2020b) nor any other model-based fuel design study has considered more than one set of fuel requirements, i.e., one engine type, and hence a comparison of optimal fuel-engine combinations on the basis of a single method has not been achieved so far. In the present study, we utilize our integrated design method (König et al., 2020b) to analyze and compare the production cost and GWI of optimized fuels for CSIEs, FFVEs, or UHEEs as shown in Figure 1. To this end, we consider a broad range of selectively-produced renewable oxygenated and non-oxygenated hydrocarbons with experimentally-proven reaction yields and fossil gasoline as an inexpensive but emission-intensive blending option. We further derive fuel requirements for all three ICE types.

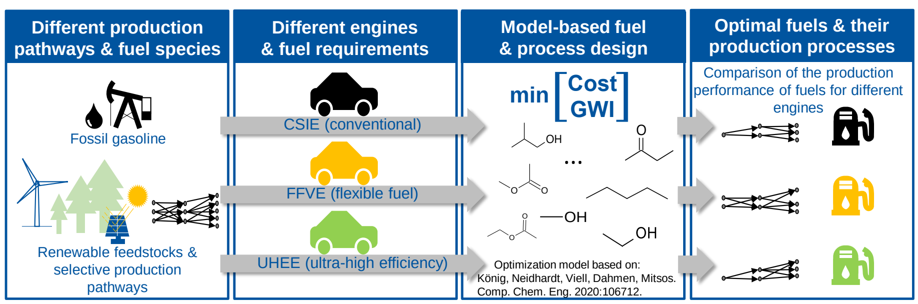

Figure 1: Scope of this study: The variety of production pathways and fuel species are inputted to an optimization problem, which considers one set of fuel requirements at a time. The optimization problem is run three times, one time for each engine type. The resulting optimal fuels for each engine type allow for a process performance comparison.

The article is structured as follows: First, we briefly review the two key parts of our optimization-based integrated design method, i.e., the pathway model and the fuel property model. Then, we give an overview of the considered fuel species and production pathways, fuel requirements, property parameters, and the structure of the optimization problem followed by the analysis of the results and a discussion section. The article ends with a conclusion.

2. Method: Integrated fuel and process design

Integrating product design with process design is a goal pursued in many domains, most prominently solvent design (Kim & Diwekar, 2002; Papadopoulos & Linke, 2006; Scheffczyk et al., 2018; Zhou et al., 2017). While integrated solvent design generally considers the product use process, in integrated fuel design, we rather consider the product manufacturing process (Villeda et al., 2012; König et al., 2020a,b).

In the present work, we use our method for integrated fuel and process design (König et al., 2020b) to optimize multi-component fuels and associated production processes for cost and GWI taking into account the fuel requirements of different ICE types. Our design method (König et al., 2020b) adapts an early-stage process screening method, i.e., Process Network Flux Analysis (PNFA) (Ulonska et al., 2016a; König et al., 2019), to evaluate not only reaction pathways but also associated downstream processing options and their energy demands, thus enabling integrated process evaluation by means of production cost and GWI estimation.

2.1. Pathway model

The pathway model adapts PNFA, a state-of-the-art process synthesis approach for early-stage process design (Ulonska et al., 2016a; König et al., 2019). In contrast to other existing process synthesis methods, which typically either conduct only mass-based analysis (Voll & Marquardt, 2012; Bao et al., 2011) or require an extensive superstructure for a more detailed process optimization (Bertran et al., 2017; Garcia & You, 2015; Kelloway & Daoutidis, 2014; Schack et al., 2020; Steimel et al., 2014) that often result in complex mixed-integer optimization problems (Friedler et al., 1998; Biegler et al., 1997), PNFA performs process design at an intermediate-fidelity level. Instead of detailed equipment sizing or optimization of the operating conditions, PNFA utilizes mole balances and energy demands to provide first estimates of cost and GWI. While PNFA has been originally developed as a simplified superstructure-based process synthesis method for lignocellulosic bio-based products (Ulonska et al., 2016a), we have recently expanded it for use in broader areas of application, i.e., bio- and electricity-based renewable fuel production (König et al., 2019). Thus, PNFA is well-suited to reliably evaluate relevant objectives for a broad range of renewable fuel production pathways, while still maintaining a screening character that allows for large-scale evaluation and optimization of these routes (Ulonska et al., 2016a; König et al., 2019).

For its process evaluation, the PNFA-based pathway model requires price and emission data, reaction pathway alternatives, stoichiometries, yields and reaction energy demands as well as the associated downstream options and their respective energy demands as input. Price and emission data as well as reaction information are taken from literature. Prior to optimization, energy requirements of reaction steps are derived based on the heat of reaction, possible latent heat changes, and the duties needed to compress gases to reaction pressure, whereas pressure changes of liquids are neglected (Ulonska et al., 2016a; König et al., 2019, 2020b). Feasible separation methods are identified using the method of Jaksland et al. (1995). The energy demands for separation of solvents and (by-)products are then determined by reduced-order separation models, most prominently Rectification Body Method (RBM) (Bausa et al., 1998; Kraemer et al., 2011), a reduced-order distillation model that determines the minimal energy demand for separation considering non-ideal thermodynamics (Ulonska et al., 2016a; König et al., 2019, 2020b). A description of all used separation models is provided in Section 4.2 of the Supplementary Material. Following our previous studies (König et al., 2019, 2020b), heat integration is considered by means of vapor recompressed distillation columns but is otherwise disregarded as it represents the last hierarchical step in process design (Douglas, 1985) and is thus considered out of scope in this early-stage process evaluation.

The pathway model includes several sets of equations, i.e., mole balances, utility demand calculations, and cost and GWI estimations. The mole balances determine the molar flow rates of all processing pathways based on the stoichiometry and yield parameters. Thus, they link product flow rates to raw material requirements. Based on the molar flow rates as well as the a priori calculated energy demands of each pathway, utility demands for steam, cooling water, refrigeration, and electricity are determined. The molar flow rates and the utility demands are used to calculate raw material cost, auxiliary cost, waste disposal cost, and utility cost using the price parameters of each cost type. Investment costs are estimated based on the total energy demands of the process using an empirical correlation by Lange (2001) that has been found to yield good predictions of biorefinery investment cost at an early process design stage (Tsagkari et al., 2016). By summing all cost types and normalizing them by a fixed fuel energy output α, the first objective function, i.e., the production cost C_{spec}, is defined. The second objective, $\mathrm{GWI}_{\mathrm{spec}}$, is calculated based on the emissions of utility and main feedstock requirements and is also normalized based on the fuel energy output α with no credit given for non-fuel by-products. The emissions of the utility (or feedstock) requirements are estimated by weighting the utility (or feedstock) requirement with the respective utility (or feedstock) emission factor. Note that we give no carbon credit to the feedstock as we assume that all products are combusted in the use/end-of-life phase, thus releasing renewable carbon back into the atmosphere. This GWI calculation corresponds to a well-to-wheel system boundary that disregards harvesting, transport, or engine efficiencies but rather focuses on emissions related to chemical processing steps (König et al., 2020b). For further descriptions of the reaction pathway modeling and economic/emission parameters the reader is referred to Section 4.1 and 4.3 of the Supplementary Material, respectively, as well as to our previous publications (König et al., 2019, 2020b).

In contrast to König et al. (2020b), we add constraints to the pathway model to allow for flexible blending ratios of fuel components even for pathways that produce multiple fuel components at a fixed ratio as, e.g., in acetone-butanol-ethanol fermentation, by considering the remaining pathway product as unused co-product. This minor modification to the pathway model is described in Section 1 of the Supplementary Material.

2.2. Fuel property model

The fuel property model is based on our previous integrated design methods (Dahmen & Marquardt, 2017; König et al., 2020b) and estimates the properties of a multi-component fuel based on pure-component fuel properties (parameters), bounds for fuel requirements (parameters), fuel composition (variables), and mixing rules (equations). Pure-component properties of each species are retrieved a priori from databases, literature, or property prediction models. The fuel requirements are derived from fuel standards in case of CSIEs and FFVEs (DIN Deutsches Institut fuer Normung e.V., 2017, 2018) and previous studies (Dahmen & Marquardt, 2017; König et al., 2020b) in case of UHEEs, which have no standardized fuel requirements, yet. The fuel composition is calculated based on the molar flow rates of the produced fuel components and thus constitutes the linking piece between the pathway model and the fuel property model. The mixing rules determine the fuel blend properties based on the fuel composition and the pure-component properties. Table 1 presents the fuel properties and the mixing rules considered in this study.

Table 1: Fuel properties and corresponding mixing rules considered in this study; NRTL: non-random two liquid.

fuel property	mixing rule
research octane number, RON [-]	linear-by-mole mixing rule (Knop et al. (2014), see Eq. S3-S4)
motor octane number, MON [-]	linear-by-mole mixing rule (Knop et al. (2014), see Eq. S3-S4)
liquid density at 15 °C, $\rho\left[\frac{\mathrm{kg}}{\mathrm{m}^3}\right]$	linear-by-weight mixing rule of specific volume (Dahmen & Marquardt, 2017; Gmehling et al., 2012; König et al., 2020b)
olefin content, olefin [vol-%]	linear-by-volume mixing rule based on liquid densities at 15 °C (see Eq. S6)
aromatic content, aromatic [vol-%]	linear-by-volume mixing rule based on liquid densities at 15 °C (see Eq. S5)
oxygen content, O_2 [wt-%]	linear-by-weight mixing rule
vapor pressure at 37.8 °C, p_{v} [kPa]	approximated by bubble point pressure with activity coefficients determined by NRTL model (Dahmen & Marquardt, 2017; König et al., 2020b; Yunus et al., 2014)
distillation curve: fuel fraction evaporated at 70 °C, 100 °C, and 150 °C, $z_{\mathrm{E70m}}, z_{\mathrm{E100m}}, z_{\mathrm{E150m}}$ [mol-%]	true boiling point curve (Eckert & Vaněk (2003); König et al. (2020b); Reiter et al. (2015), see Eq. S7)
surface tension at 25 °C, $\sigma\left[\frac{\mathrm{mN}}{\mathrm{m}}\right]$	Parachor-based mixing rule (Dahmen & Marquardt, 2017; Gmehling et al., 2012; König et al., 2020b)
kinematic viscosity at 25 °C, $\nu\left[\frac{\mathrm{mm}^2}{\mathrm{s}}\right]$	linear-by-mole mixing rule for dynamic viscosity (Dahmen & Marquardt, 2017; Gmehling et al., 2012; König et al., 2020b)
enthalpy of vaporization at 25 °C, $H_{\mathrm{vap}}\left[\frac{\mathrm{kJ}}{\mathrm{kg}_{\mathrm{air},\Phi=1}}\right]$	linear-by-weight mixing rule (Chupka et al., 2015; Dahmen & Marquardt, 2017; König et al., 2020b)

Compared to König et al. (2020b), we amend the list of considered fuel properties such that they account for key aspects of the current European E10 and E85 gasoline standards, i.e., EN228 and EN15293 (DIN Deutsches Institut fuer Normung e.V., 2017, 2018), for CSIEs and FFVEs, respectively. Instead of the previously used derived cetane number (DCN), we use research octane number (RON) (International Organization for Standardization, 2014b) and motor octane number (MON) (International Organization for Standardization, 2014a) as indicators for knock resistance. Furthermore, we consider density and oxygen content as fuel properties that, in combination, ensure a sufficiently high calorific heating value. We further use olefin and aromatic content as standardized fuel properties. Similar to our previous studies (Dahmen & Marquardt, 2017; König et al., 2020b), we describe the volatility of the fuel by means of the vapor pressure and the distillation curve with the latter being modeled by the true boiling point (TBP) concept (Eckert & Vaněk, 2003; Reiter et al., 2015). In addition to these standardized fuel properties, we adopt surface tension, kinematic viscosity, and enthalpy of vaporization as relevant fuel properties for UHEEs (Dahmen & Marquardt, 2017; Hoppe et al., 2015; König et al., 2020b). With regard to the fuel distillation curve, the EN228 standard (DIN Deutsches Institut fuer Normung e.V., 2017) restricts the evaporated fuel fractions at certain temperatures whereas the ASTM standard (ASTM D4814, 2020) limits the temperature range at a certain evaporated fuel fraction. The advantage of considering the former instead of the latter standard is that our TBP model does not need binary variables. Compared to our previous study, where we used the ASTM fuel standard, consideration of the EN228 standard simplifies the optimization problem to a continuous nonlinear program (NLP), which is easier to solve than the previous mixed-integer nonlinear program. The details of the TBP model formulation and a description of the new mixing rules for RON, MON, olefin and aromatic content are given in Section 2 of the Supplementary Material. All other mixing rules are directly taken from König et al. (2020b).

3. Optimizing fuels and associated production routes for UHEEs, FFVEs, and CSIEs

Prior to pathway and fuel optimization, we pre-screen 71 renewable fuel candidates based on their pure-component properties and current purchase cost. The renewable fuel species that pass pre-screening are forwarded to integrated fuel and process design along with their production routes and a gasoline surrogate. In the following, the pre-screening, the pathway model parameters, the fuel property model parameters, and the optimization problem are described.

3.1. Pre-screening of fuel candidates

In contrast to previous fuel design studies, which have mostly focused on a relatively small number of renewable fuel species (Ariffin Kashinath et al., 2012; Yunus et al., 2014; Hashim et al., 2017; Kalakul et al., 2018; König et al., 2020b), we consider an initial set of 71 renewable, selectively-produced species in this study. More specifically, we consider 50 fuel candidates evaluated in a recent review by Gschwend et al. (2019), 13 additional fuel candidates from one of our previous integrated design study (Dahmen & Marquardt, 2017), and 8 additional non-oxygenated candidates found by reviewing an octane number compendium (Derfer et al., 1958) and identifying one or multiple corresponding renewable production pathways by a thorough literature review assisted by reaction databases (Elsevier Information Systems GmbH, 2020; American Chemical Society, 2020). For an overview of the pre-screened species, the reader is referred to Table S1 of the Supplementary Material. Based on these 71 candidates, we conduct a pre-screening that eliminates unsuitable species based on pure-component volatility, toxicity, and current purchase price.

For volatility, the pure-component normal boiling point (NBP) serves as a facile pre-screening criterion since it is readily available from databases. We apply a lower limit of 30 °C for the NBP to ensure that each fuel candidate is liquid at ambient temperatures and can thus easily be mixed in a lab. As an upper bound on the NBP, we use the final SI engine boiling point restriction of the distillation curve, i.e., 210 °C (DIN Deutsches Institut fuer Normung e.V., 2017).

Next, we exclude fuel candidates with known high toxicity based on the LC50 of rats inhaling fuel vapor. Fuel candidates with a vapor-based LC50 value below 10 $\frac{\mathrm{mg}}{\mathrm{L} \cdot 4\mathrm{hr}}$ are categorized as toxic or even fatal (SCHC-OSHA Alliance GHS/HazCom Information Sheet Workgroup, 2017). Thus, we remove them from further analysis to contribute to safer handling in future fuel testing or application. For comparison, a light naphtha gasoline has an LC50 value of 20.7 $\frac{\mathrm{mg}}{\mathrm{L} \cdot 4\mathrm{hr}}$ (Everhart & Hoover - Power Line Construction, Inc, 2020), which qualifies as harmful but not toxic (SCHC-OSHA Alliance GHS/HazCom Information Sheet Workgroup, 2017) and would therefore pass the pre-screening.

Lastly, we discard fuel candidates that can currently not be commercially purchased or only at high prices of more than 200 $\frac{\mathrm{EUR}}{\mathrm{L}}$. Even though this pre-screening criterion represents a strong limitation, setting a price limit is necessary to practically enable future experimental testing of the designed fuels.

3.2. Pathway model parameters

Figure 2 shows a graphical representation of the reaction pathway alternatives for the renewable fuel species considered in optimization. Renewable fuel species can be produced from lignocellulosic biomass, renewable H_2, and/or CO_2 via various intermediates.

We take reaction pathway data from literature and design/calculate the downstream processing options using separation models (Aspen Technology, 2015; Bausa et al., 1998; Kraemer et al., 2011). For some fuel species, pathway data can be taken from previous studies (Dahmen & Marquardt, 2017; König et al., 2019, 2020b; Ulonska et al., 2016a). For the other fuel components, we first identify appropriate pathways that connect the feedstocks to the fuel species by conducting a manual literature research assisted by the use of reaction databases (Elsevier Information Systems GmbH, 2020; American Chemical Society, 2020). Using, e.g., the "synthesize" option of Reaxys, over 53 million chemical reactions are screened and an exhaustive overview of reactions leading

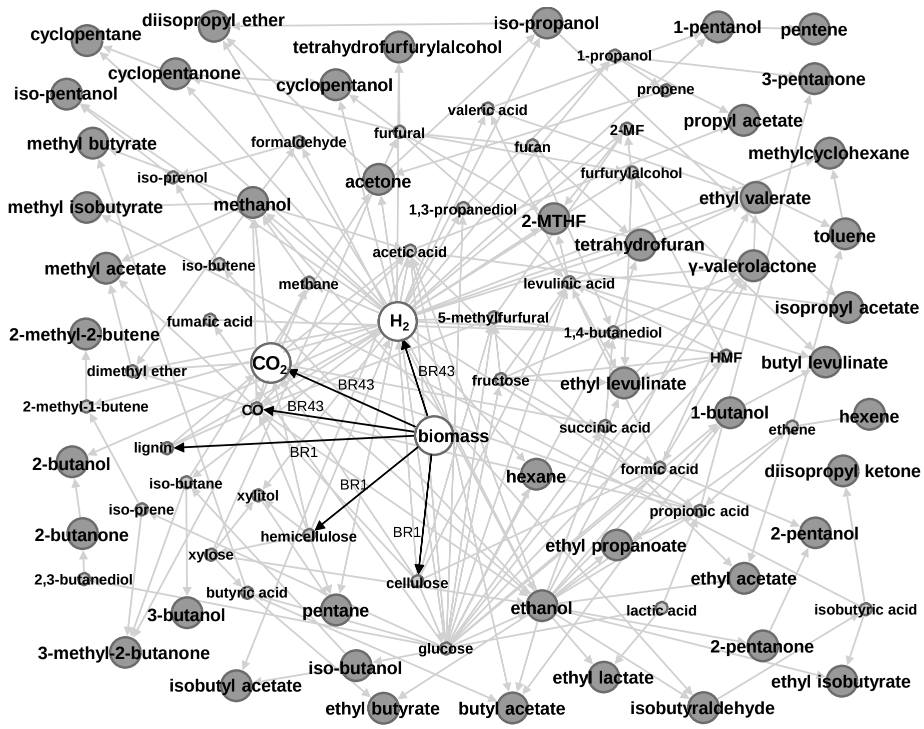

Figure 2: Overview of renewable fuel species and their production pathways considered during optimization. Fuel species (large, dark gray nodes) are produced via various intermediates (small, light gray nodes) from lignocellulosic biomass, renewable H_2, and/or CO_2 (large white nodes). Edges indicate reaction pathways; initial biomass conversion pathways, i.e., BR1 and BR43, are exemplarily highlighted. Mixing/separation steps as well as auxiliaries are omitted. 2-MTHF: 2-methyltetrahydrofuran; HMF: 5-hydroxymethylfurfural; 2-MF: 2-methylfuran.

to a specified fuel species is given. Based on these database results, we identify suitable reactions leading from renewable feedstocks or platform molecules towards the final fuel molecule. Longer routes with a multitude of intermediates are more difficult to identify as the number of reactions and species to research strongly increases. However, as such long routes are typically also associated to higher yield losses and increased separation efforts, our focus on short routes is not expected to affect the optimization results. To ensure that the network is exhaustive, network generators such as RING (Rangarajan et al., 2010, 2012, 2014) could be used in the future. However, completely switching to such automated rule-based methods comes at the cost of losing experimental yield and process information, which is needed for a thorough cost and GWI estimation. All reaction pathway and downstream processing data can be found in Tables S2-S15 of the Supplementary Material.

The initial biomass conversion routes are highlighted in Figure 2. They include a generic pretreatment step for biomass fractionation (BR1) (Ulonska et al., 2016a) and biomass gasification (BR43) (Gil et al., 1999; König et al., 2019). After fractionation (BR1), cellulose and hemicellulose can be hydrolyzed to sugars (modeled as glucose and xylose, respectively) (Manonmani & Sreekantiah, 1987; König et al., 2019; Ulonska et al., 2016a), gasified (Gil et al., 1999; König et al., 2019), or directly converted into other species. Based on glucose and xylose, a wide range of fuel species can be produced via catalytic and fermentative routes. The third biomass fraction, lignin, however, is considered for gasification only (Gil et al., 1999; König et al., 2019).

The literature pathway data and their respective energy demands are used for cost and GWI calculation as described in Section 2.1. To this end, the pathway model further requires price data of all feedstocks and auxiliaries, economic parameters for investment cost calculations, and emission data of utilities and main feedstocks. In the following, a brief description of the emissions and the prices of the main feedstocks, i.e., gasoline, biomass, H_2, and CO_2, is given. For gasoline, which is modeled by an eight-component surrogate from Sarathy et al. (2016), we assume a price of 0.38 $\frac{\text{USD}}{\text{kg}_{\text{gasoline}}}$, which is equivalent to the average German tax-free retail price of gasoline in 2016 (European Commission, 2016), and an emission factor of 4.05 $\frac{\text{kg}_{\text{CO2,eq.}}}{\text{kg}_{\text{gasoline}}}$, which equals the EU fossil fuel comparator value of 94 $\frac{\text{kg}_{\text{CO2,eq.}}}{\text{GJ}_{\text{gasoline}}}$ (European Parliament and the Council of the European Union, 2018). For lignocellulosic biomass, we assume a composition based on beech wood, i.e., 47.7 mol-% cellulose (approximated as $C_6H_{10}O_5$), 35.1 mol-% hemicellulose (approximated as $C_5H_{10}O_5$), and 17.2 mol-% lignin (approximated as $C_{10}H_{12}O_3$) (Couhert et al., 2009; Dahmen & Marquardt, 2017), and a price of 50 $\frac{\text{USD}}{\text{ton}_{\text{biomass}}}$ (Ruth, 2011). We disregard upstream emissions of biomass, e.g., for harvesting and transport, since the focus of this study is strictly on the conversion process. The second renewable feedstock, H_2, is provided to our process at steady-state at a price of 5.8 $\frac{\text{USD}}{\text{kg}_{\text{H2}}}$ (Grube & Höhlein, 2014). Based on the emissions of off-shore wind power in 2020 (International Institute for Sustainability Analysis and Strategy, 2015) and the electricity demand of electrolysis (Götz et al., 2016), the emissions caused by water electrolysis are incorporated as 0.256 $\frac{\text{kg}_{\text{CO2,eq.}}}{\text{kg}_{\text{H2}}}$. For the third renewable feedstock, CO_2, we assume production via carbon capture from a steel plant exhaust gas stream at upstream emissions of 0.034 $\frac{\text{kg}_{\text{CO2,eq.}}}{\text{kg}_{\text{CO2}}}$ (Kasten et al., 2013; International Institute for Sustainability Analysis and Strategy, 2015) and cost of 40 $\frac{\text{USD}}{\text{ton}_{\text{CO2}}}$ (Quader et al., 2016; König et al., 2019). A complete overview of all cost and emission parameters is provided in Tables S16-S18 of the Supplementary Material.

Finally, we assume a fixed fuel output of $\alpha = 2.77 \cdot 10^{12} \frac{\text{kJ}}{\text{yr}}$. This value is equal to the fuel output used in our previous studies (König et al., 2020b, 2019; Ulonska et al., 2016a) and roughly relates to the energy content of 100,000 $\frac{\text{tons}_{\text{ethanol}}}{\text{yr}}$.

3.3. Fuel property model parameters

The fuel property model requires pure-component data for all species and a set of fuel requirements for each ICE type. We take the pure-component fuel properties from databases and literature or use property prediction models. We adapt fuel requirements from European fuel standards (DIN Deutsches Institut fuer Normung e.V., 2017, 2018) and from our previous studies (Dahmen & Marquardt, 2017; König et al., 2020b). In the following, the compiled data, their sources, and assumptions are described in more detail.

We take experimental pure-component RON and MON data from literature (Derfer et al., 1958; Yanowitz et al., 2011; McCormick et al., 2017; Naegeli et al., 1989; Lange et al., 2010). For those fuels, for which no experimental data is available, we estimate the RON and MON values using our recently developed data-driven approach that predicts RON and MON based on the molecular graph (Schweidtmann et al., 2020). We use the DIPPR database to retrieve pure-component data for liquid density, kinematic viscosity, surface tension, and enthalpy of vaporization (AIChE, 2018). For species not included in the DIPPR database, we use experimental values from other sources listed in Tables S20-S22 of the Supplementary Material. Finally, the calculation of the fuel vapor pressure requires pure-component vapor pressures at 37.8 °C and parameters to calculate activity coefficients. For pure-component vapor pressures, we use the extended Antoine equation with parameters taken from Aspen Plus (Aspen Technology, 2015), or from vapor pressure handbooks (Yaws & Satyro, 2015; Hall, 2000). To calculate the activity coefficients during optimization, we apply the non-random two liquid (NRTL) model (Renon & Prausnitz, 1968) with parameters fitted to activity coefficients predicted by COSMO-RS (Klamt, 2019). An overview of all pure-component fuel properties is provided in Tables S19-S22 of the Supplementary Material.

We consider three sets of fuel requirements that describe key specifications for the three different engine types, i.e., CSIEs, FFVEs, and UHEEs. The fuel requirements are shown in Table 2.

Table 2: Fuel requirements for the three engine types considered in this study: CSIE (based on EN228 DIN Deutsches Institut fuer Normung e.V. (2017)), FFVE (based on EN15293 DIN Deutsches Institut fuer Normung e.V. (2018)), and UHEE (based on previous studies by König et al. (2020b); Dahmen & Marquardt (2017)). Dash denotes no restriction; parentheses denote generic restrictions given to the optimizer.

	min			max		
	CSIE	FFVE	UHEE	CSIE	FFVE	UHEE
research octane number, RON [-]	95	95	110	(150)	(150)	(150)
motor octane number, MON [-]	85	85	-	(150)	(150)	-
liquid density at 15 °C, ρ $\left[\frac{\mathrm{kg}}{\mathrm{m}^3}\right]$	720	720	-	775	800	-
olefin content, olefin [vol-%]	(0)	(0)	(0)	18	18	18
aromatic content, aromatic [vol-%]	(0)	(0)	(0)	35	35	35
oxygen content O_2 [wt-%]	(0)	-	10	3.7	-	(100)
vapor pressure at 37.8 °C p_v [kPa]	45	35	35	100	100	100
E70 distillation fraction $z_{70\mathrm{m}}$ [mol-%]	22	3	3	52	52	52
E100 distillation fraction $z_{100\mathrm{m}}$ [mol-%]	46	46	46	72	(100)	(100)
E150 distillation fraction $z_{150\mathrm{m}}$ [mol-%]	75	75	75	(100)	(100)	(100)
surface tension at 25 °C, σ $\left[\frac{\mathrm{mN}}{\mathrm{m}}\right]$	-	-	(0)	-	-	30
kinematic viscosity at 25 °C, ν $\left[\frac{\mathrm{mm}^2}{\mathrm{s}}\right]$	-	-	0.5	-	-	2
enthalpy of vaporization at 25 °C, H_vap $\left[\frac{\mathrm{kJ}}{\mathrm{kg}_{\mathrm{air},\Phi=1}}\right]$	-	-	(0)	-	-	60

The fuel requirements for CSIEs are based on the EN228 gasoline standard for E10 gasoline (DIN Deutsches Institut fuer Normung e.V., 2017). The restrictions on RON and MON, liquid density, vapor pressure, and content of olefins, aromatics, and oxygen are directly taken from the EN228 standard (DIN Deutsches Institut fuer Normung e.V., 2017). The EN228 standard is also the basis for the distillation curve restrictions. However, instead of volume fractions, we assume mole fractions as these allow for a simpler and more efficient model formulation. In our previous study (Dahmen & Marquardt, 2017), the simplification to mole-based distillation curves only caused small deviations in comparison to a volume-based modeling approach.

For FFVEs, we expand the fuel requirements used for CSIEs by considering the EN15293 standard for E85 fuel (DIN Deutsches Institut fuer Normung e.V., 2018). Note that FFVEs can operate on both regular gasoline and E85 fuel (Ford Motor Company, 2020). Following the EN15293, we choose a maximal allowed density of 800 $\frac{\mathrm{kg}}{\mathrm{m}^3}$, eliminate O_2 content restrictions, and set the lower bound for the vapor pressure to 35 kPa. As the distillation curve is not explicitly addressed by the EN15293 standard, we expand the corresponding restrictions based on the distillation curve of a typical E85 fuel (Andersen et al., 2010).

We stress that our CSIE and FFVE fuel requirements disregard further standardized properties. Most importantly, we neglect restrictions on specific oxygenates, e.g., methanol, since limiting our study to the few oxygenates explicitly named in the standard would defeat most purpose of fuel design. We postpone analysis of corrosion effects and oxidation stability to future blend validation due to the lack of suitable models. We consider the vapor pressure and distillation curve restrictions to be sufficient indicators for volatility and thus disregard the vapor lock index. Finally, we exclude restrictions on impurities, e.g., benzene, manganese, water, and lead content, as they do not apply to our study.

For UHEEs, which are not yet commercially available, we adapt the fuel requirements defined in our earlier study (König et al., 2020b). Instead of using DCN as a surrogate parameter for RON, we now directly consider RON to assess fuel knock resistance. Since DCN and RON are inversely correlated, the previously employed restriction, DCN $\leq$ 10, can be roughly translated into a new restriction of RON $\geq$ 110 (Perez & Boehman, 2012). Such high RONs indicate strong anti-knock behavior even under the extreme operating conditions of UHEEs. Aiming at uniform mixture formation and resulting clean combustion, the surface tension and viscosity are restricted. Moreover, a lower bound is used for the O_2 content to limit soot formation (König et al., 2020b; Dahmen & Marquardt, 2017). To reduce harmful engine-out emissions that can arise due to olefins and aromatics (Karavalakis et al., 2015; Wei et al., 2019), we restrict their respective contents based on the EN228 standards (DIN Deutsches Institut fuer Normung e.V., 2017). We set the restrictions on distillation curve and vapor pressure for UHEEs equal to those of FFVEs. As an additional indicator for mixture formation during cold-start/-run phases, the UHEE-based fuel requirements include the enthalpy of vaporization (König et al., 2020b). As in König et al. (2020b), the UHEE-based fuel requirements do not consider a limit on the MON or the fuel density, thus leaving those fields of Table 2 blank.

3.4. Overview of the nonlinear optimization problem

We implement the multi-objective continuous NLP in GAMS version 30.1 (GAMS Development Corporation, 2020) using the ϵ-constraint method (Haimes et al., 1971). For each ICE type, pathway model and fuel property model are solved simultaneously considering the respective fuel requirements of Table 2 and using the deterministic global solver BARON version 19.12.7 (Khajavirad & Sahinidis, 2018). We set a branching priority of 20 on the molar fuel fractions. Furthermore, we assign a relative optimality tolerance of 0.01 and a time limit of 6000 seconds to each optimization run. While for some runs, e.g., those for CSIE fuels, a guaranteed global solution is found, for others, the time limit is reached before the problem has converged to the desired optimality. When we tried solving times larger than 6000 seconds, no better solution was found but instead, we have observed that the lower bound convergence stagnates. Furthermore, in all cases, we have seen that all branchand-bound iterations only alter the lower bound, whereas the upper bound does not improve after BARON's pre-processing. We thus presume that the solution found is indeed globally optimal. The complete nonlinear optimization problem is summarized below. For the specific equations, the reader is referred to König et al. (2020b) and the Supplementary Material:

$$\min \begin{bmatrix} \text{specific cost, } C_{\text{spec}} \\ \text{specific GWI, } \text{GWI}_{\text{spec}} \end{bmatrix}$$

s.t. pathway model

product and side product mole balances and yield restrictions,

utility requirements of reaction/separation pathways,

raw material cost,

waste disposal cost,

utility cost,

investment cost,

process- and feedstock-related GWI estimation,

fixed annual fuel output α,

molar flow rates of fuel species put in blend (Eq. S1-S2),

fuel property model

mole and mass fractions of fuel,

mixing rule for RON and MON (Eq. S3),

mixing rule for density,

mixing rule for aromatic and olefin content (Eq. S5-S6),

oxygen content of fuel,

mixing rule for viscosity,

mixing rule for surface tension,

mixing rule for enthalpy of vaporization,

calculation of vapor pressure,

TBP curve: mole fraction of fuel evaporated at 70, 100, and 150°C (Eq. S7),

lower and upper bounds of fuel properties according to fuel requirements,

nonnegativity constraints for fluxes.

To provide further insights on cost and GWI of the production of each fuel species, we also optimize the pathway model for each fuel species individually without taking into account any fuel requirements (see Section 6 of the Supplementary Material for the results).

4. Results

The pre-screening reduces the initial number of 71 possible fuel candidates based on three criteria (see Section 3.1). The first screening criterion (NBP) leaves 66 suitable species. The second criterion (LC50) reduces the number further to 57 candidates and finally, the third criterion (current purchase price) leaves 47 renewable fuel species and their production pathways (see Figure 2), which are forwarded to the optimization problem.

Optimization of the considered 47 renewable fuel species, their production pathways, and a gasoline surrogate yields the fuel production performances, compositions, and properties given in Figure 3. The left diagrams show the Pareto fronts for cost and GWI optimization. Each point on each of the Pareto fronts corresponds to a Pareto-optimal fuel and process design. The optimal fuel compositions are given in the centered bar charts. The corresponding optimal pathway designs are summarized in Table S23 of the Supplementary Material. Finally, the right diagrams of Figure 3 show the properties of the respective optimal fuels with their axes being normalized to the minimal and maximal allowed values for each property and engine type (see values in Table 2).

The Pareto fronts (left part of Figure 3) provide the performance comparison between the optimized fuels with the direction of optimization pointing towards the origin of the graph. As expected, fossil gasoline remains the least costly fuel and is thus chosen by the optimizer as the cost-optimal CSIE and FFVE fuel. For UHEE fuels, which require a minimum oxygen content of 10 wt-% and a minimum RON of 110 (see Table 2), gasoline alone is not feasible but highly knock-resistant oxygenates like methyl acetate are blended. As GWI is reduced, the content of renewable fuels increases for all ICE types. At the point of minimal GWI, all optimized fuels are completely renewable. CSIE fuels

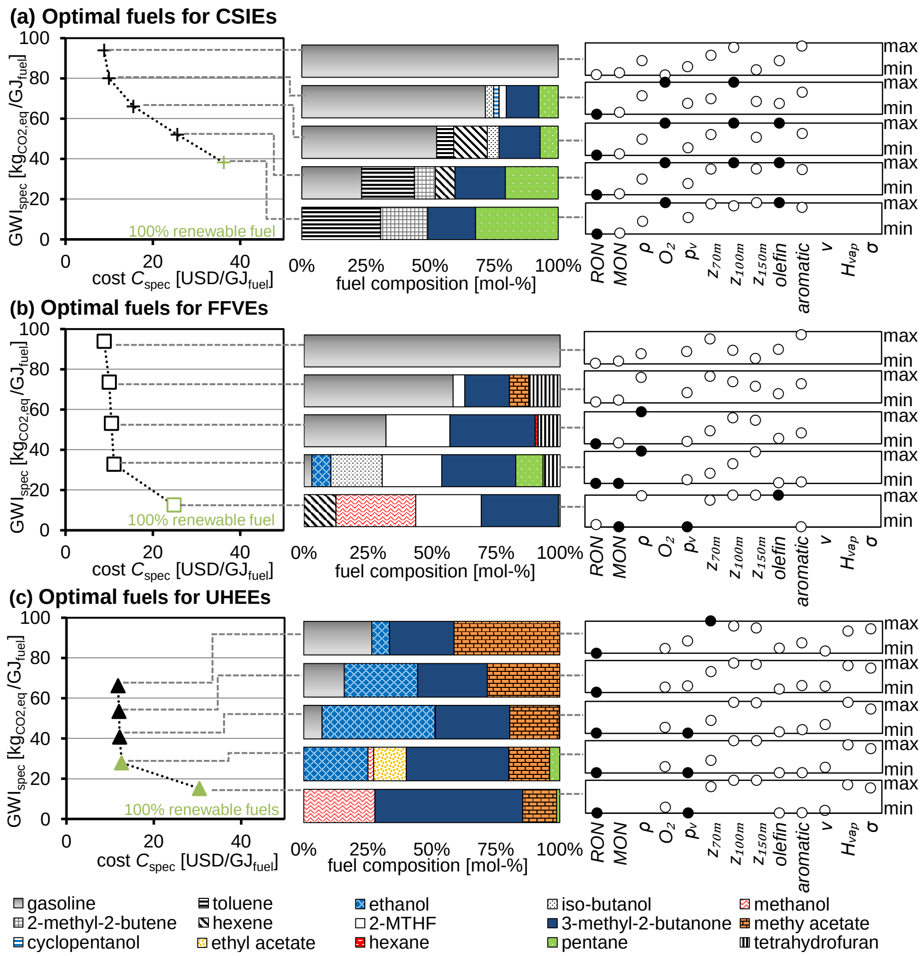

Figure 3: Optimized fuels for (a) CSIEs (commercialized), (b) FFVEs (commercialized), and (c) UHEEs (future engines subject to further development): The left diagrams present the Pareto fronts for cost and GWI optimization. The bar charts in the center show the optimal fuel compositions, and the right charts display the respective fuel properties with black points indicating a limiting fuel requirement, white points referring to a specified but non-limiting fuel requirement and blank spaces showing that the fuel property is not restricted for the respective engine (see Table 2 for values of minimal and maximal bounds as well as symbols used in right diagram).

show a comparatively high GWI of 38 $\frac{\mathrm{kg}_{\mathrm{CO2,eq}}}{\mathrm{GJ}_{\mathrm{fuel}}}$ at the point of minimal GWI and high cost. In contrast, GWI-optimal fuels for UHEEs and FFVEs reach GWIs reductions of up to 84% and 87%, respectively, compared to regular gasoline. Such GWI reductions also incur high cost, which are, however, smaller than those of CSIE fuels. As the Pareto fronts of FFVE and UHEE fuels are generally located closer to the lower left corner of the graph, it can be concluded that they have better Pareto performance compared to the CSIE fuels.

The differences in cost and GWI performance trace back to the different fuel requirements. More specifically, as CSIE fuels are limited to a maximum O_2 content of 3.7 wt-% (DIN Deutsches Institut fuer Normung e.V., 2017), they cannot take as much advantage of low-cost, low-GWI oxygenates as FFVE and UHEE fuels. Instead, hydrocarbons like hexene or pentane are added, which can be produced at relatively low GWI and low cost but are subject to unfavorable knocking characteristics, i.e., $\mathrm{RON}_{\mathrm{pentane}}$=62, $\mathrm{RON}_{\mathrm{hexene}}$=76 (Derfer et al., 1958). As a result, RON arises as another limitation next to O_2 content (see upper right diagram in Figure 3). The low RON of pentane and hexene is counteracted by blending of the knock-resistant hydrocarbon toluene with $\mathrm{RON}_{\mathrm{toluene}}$=120 (Derfer et al., 1958). Toluene, however, is produced via a rather long production route that incurs many yield losses leading to high raw material and waste costs. The unfavorable production performance of non-oxygenates like toluene explains the rather flat shape of the CSIE fuel Pareto front.

FFVEs allow for more flexibility in fuel design as their fuel requirements are adapted to a high fuel oxygen content (see Table 2). Next to fossil gasoline, low-cost, low-GWI renewable oxygenates like 3-methyl-2-butanone, 2-methyltetrahydrofuran (2-MTHF), and tetrahydrofuran are blended in the optimal fuels (see central composition diagram in Figure 3). At lower GWIs, the content of renewable fuel species increases giving rise to property limitations, e.g., due to the unfavorable knocking characteristics of the two tetrahydrofurans. Furthermore, the density and vapor pressure are restricted to a maximum of 800 $\frac{\mathrm{kg}}{\mathrm{m}^3}$ and a minimum of 35 kPa, respectively (DIN Deutsches Institut fuer Normung e.V., 2018). These limits are violated by many oxygenates and therefore also pose limitations at high renewable fuel contents (see center right diagram in Figure 3).

UHEE fuels are not limited by an upper O_2 content or density but must have a minimum RON of 110 (see Table 2). Thus, highly knock-resistant species like methyl and ethyl acetate or methanol and ethanol are added (see center lower diagram in Figure 3). The blending of alcohols may lead to problematic cold-start operation (Markel & Bailey, 1998). In our designs, we use the vapor pressure and enthalpy of vaporization constraints to limit this well-known unfavorable property of the alcohols. This results in blending of either fossil gasoline or renewable pentane (see lower centered diagram in Figure 3).

We observe that, irrespective of the ICE type, some fuel components are blended more often than others indicating that their production either shows favorable cost and GWI or that they complement other species that show favorable cost and GWI. To provide further insights on cost and GWI of the production of each fuel species, we optimize the pathway model for each fuel species individually without taking into account any fuel requirements. The results of this analysis are given in Figure S1 and Table S24 of the Supplementary Material. While individual production cost and GWI do not account for co-production benefits, the results still help to understand why, e.g., pentane and 3-methyl-2-butanone emerge as blending candidates of first choice (see center diagrams of Figure 3). Specifically, 3-methyl-2-butanone is produced from the cellulose fraction of biomass via the intermediate iso-prene that can be recovered from the aqueous phase using simple phase separation. This facile separation, the use of inexpensive biomass feedstock, and the high RON make 3-methyl-2-butanone an attractive low-cost, low-GWI fuel component (see Figure S1(b) of the Supplementary Material). In contrast, pentane is produced from the hemicellulose fraction via xylitol. Again, the downstream processing exploits a miscibility gap leading to low emissions. Even though there are other fuel species with an even better individual production performance than pentane (see Figure S1 of the Supplementary Material), the use of the hemicellulose fraction is complementary to the production of many C_6-based fuel species. Furthermore, the low density, high volatility, and the lack of an oxygen atom make pentane an interesting blending candidate that balances well with many oxygenates including

3-methyl-2-butanone.

To illustrate how 3-methyl-2-butanone and pentane are produced in an overall process, we consider the 100%-renewable, low-cost, low-GWI UHEE fuel that shows cost of 13 $\frac{\mathrm{USD}}{\mathrm{GJ_{fuel}}}$ and a GWI of 28 $\frac{\mathrm{kg_{CO2,eq}}}{\mathrm{GJ_{fuel}}}$ in the UHEE Pareto front in Figure 3(c). This fuel is produced by the production routes seen in Figure 4. First, biomass feedstock is fractionated into cellulose, hemicellulose, and lignin (BR1). Then, the cellulose fraction is converted to low-cost, low-GWI 3-methyl-2-butanone via glucose and iso-prene intermediates (BR264, BR255) whereas hemicellulose is used to produce multiple species, i.e., ethanol (BR4, BR7), ethyl acetate (BR4, BR7, BR116), and pentane (BR320, BR273). Ethanol, which has a RON of 109 (Yanowitz et al., 2011), can be produced at relatively low cost and low GWI (see Figure S1(a)) and ethyl acetate acts as an octane booster with a RON of 118 (McCormick et al., 2017). The production of ethyl acetate via BR116 also co-produces H_2, which is used as an auxiliary input for the production of pentane that increases the volatility of the fuel and hence ensures a feasible vapor pressure. As the co-produced H_2 from BR116 is not sufficient for pentane production, additional H_2 is provided by syngas (modeled as a mixture of CO, H_2, and CO_2) from lignin gasification (BR46). The syngas is also used in HR5, HR16, and BR123 to produce methanol and methyl acetate, respectively. Methyl acetate, which has an exceptional RON of 120 (McCormick et al., 2017), enhances knock-resistance whereas methanol has a better process performance due to the shorter pathway. This integrated use of lignin-based syngas and co-produced H_2 from BR116 avoids external provision of expensive electricity-based H_2. External CO_2 is also not required since enough CO_2 for HR16 is co-produced during syngas treatment and further CO_2 from ethanol and iso-prene fermentation (BR7, BR264) is even left unused. This exemplary process shows how different fuel species can be efficiently co-produced to yield a fully renewable UHEE blend that not only fulfills the fuel requirements but also leads to high GWI reductions at relatively small cost increases compared to fossil gasoline.

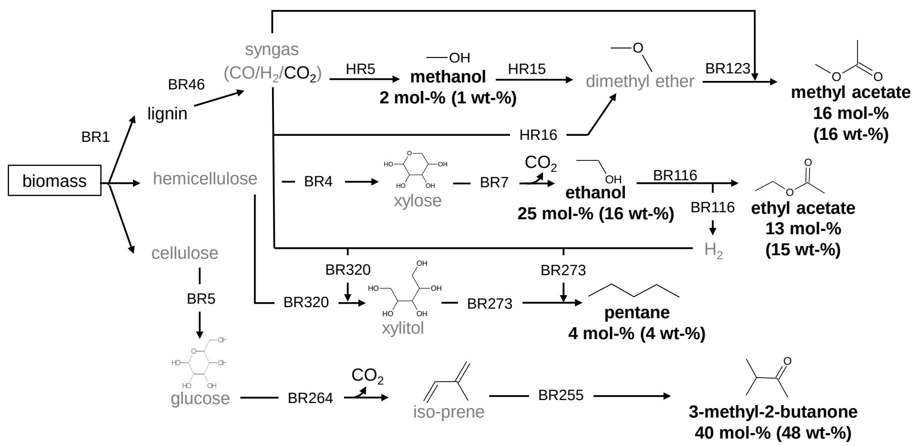

Figure 4: Optimal processing scheme for exemplary UHEE fuel (corresponding process performance of 13 $\frac{\mathrm{USD}}{\mathrm{GJ}_{\mathrm{fuel}}}$ and 28 $\frac{\mathrm{kg}_{\mathrm{CO2,eq}}}{\mathrm{GJ}_{\mathrm{fuel}}}$ is seen in the UHEE Pareto front in Figure 3(c)). Externally provided feedstock, i.e., biomass, is indicated by a black-lined box. Gray font indicates intermediates that are produced but fully converted into other species. Bold black font refers to species that are added to the blend with the indicated percentages given in mol-% and, alternatively, wt-%. Normal black font denotes species that are co-produced. Auxiliary reactants and products, e.g., water, are omitted along with all separation steps in this visualization.

5. Discussion

This study optimizes fuels for different ICE types regarding production cost and GWI taking into account a wide range of alternative fuel species and associated production pathways. While fossil gasoline is still the least costly fuel, 100% renewable fuels are designed for all engine types at minimal GWI. The design of 100% renewable, selectively-produced CSIE fuels constitutes a significant improvement over many previous model-based CSIE fuel designs, which only achieve moderate amounts of renewable fuel content (Marvin et al., 2013; Yunus et al., 2014). This is mainly due to the fact that our study includes a wide variety of oxygenated and non-oxygenated fuel species allowing for more complex mixtures to be designed without the need of fossil gasoline blending. For the relatively new concept of UHEEs, fully renewable fuel blends are feasible by design and have already been formulated in our previous studies (Dahmen

& Marquardt, 2017; König et al., 2020b). However, compared to Dahmen & Marquardt (2017), our pre-screening step (see Section 3.1) eliminates all gaseous and commercially unavailable species, thus simplifying future experimental research. Furthermore, our designed UHEE fuels provide both cost and GWI improvements compared to the UHEE fuels designed in König et al. (2020b). This is again due the large scope of this study, which includes a gasoline surrogate as well as 47 renewable fuel species, some with very promising process performance, whereas our previous study only included a proof-of-concept case study with 7 renewable fuel species (König et al., 2020b).

By conducting an integrated fuel design for several engine types, i.e., CSIEs, FFVEs, and UHEEs, this study allows for a comparison of the process cost and GWI reduction potentials of optimized, selectively-produced fuels for different ICE types. Based on the three sets of fuel requirements derived in this study, the results show that for all considered ICE types, GWI reduction potentials of 60% are possible through renewable fuel production. For CSIE fuels, these GWI reductions are associated to high production costs, whereas FFVE and UHEE fuels achieve the same GWI reduction at nearly the same cost as fossil gasoline. Moreover, FFVE and UHEE fuels can achieve further GWI reductions of up to 87% and 84% compared to fossil gasoline, respectively. For example, the 100%-renewable UHEE fuel that is produced via the production routes seen in Figure 4 reduces GWI by 70% with relatively small cost increases compared to fossil gasoline (see Figure 3). These cost increases are estimated to lie within ranges that could be compensated by tax reductions on renewable fuels (European Commission, 2016). Furthermore, the estimated GWI reductions of 70% meet the current European CO_2 reduction targets for biofuels, i.e., 65% reduction for plants starting production in 2021 or later (European Parliament and the Council of the European Union, 2018). Similar cost and GWI performances can be achieved with an designed FFVE fuel that contains small contents of fossil gasoline.

The designed fuels should be experimentally tested with respect to engine compatibility. For FFVEs and CSIEs, we considered many important properties standardized in Europe but had to disregard others (see Section 3.3) thus clearly leading to a best-case assessment. However, even under such idealizing assumptions, our results suggest an unfavorable cost/GWI Pareto performance of optimized fuels for CSIEs with the main fuel property bottleneck being the strongly restricted oxygen content that renders the extensive use of many efficient pathways leading to oxygenated species infeasible. These results are based on selective, experimentally-proven production routes. In principle, incorporating unselective production routes such as pyrolysis or the Fischer-Tropsch process that yield non-oxygenated hydrocarbon mixtures could improve the performance of optimized CSIE fuels.

The superior process performance of selectively-produced FFVE and UHEE fuels provides an argument for switching from today's CSIE technology to advanced engine technologies. In the future, this supposed benefit in fuel production should be weighed against the investments in technology development, market launch, and fuel distribution infrastructure that are needed for large-scale implementation of FFVEs or UHEEs and their respective fuels. FFVEs are already commercially available (Ford Motor Company, 2020) thus enabling a potentially faster and less costly change than the implementation of UHEEs, which are still in research phase. Furthermore, FFVEs have the potential to enable a smooth transition from fossil fuels to renewable ones since they are suited for both types of fuels and hence can also be used during a transitional phase, in which the fueling station infrastructure of renewable fuels is limited. In comparison, regular gasoline is not feasible in UHEEs, which require fuels with higher knock-resistance, thus leading to a stronger market entry barrier. The large-scale implementation of UHEEs therefore requires more time and effort but promises cleaner and more efficient combustion compared to the current engine technology (Hoppe et al., 2015). To quantify this benefit, fuel-specific engine efficiency and engine-out pollutant emissions need to be determined and co-optimized in future comparisons.

6. Conclusion

This study quantifies and compares cost and GWI reduction potentials of fuels for CSIEs, FFVEs, and UHEEs. To this end, we conduct a pre-screening of 71 fuel candidates and apply our model-based integrated fuel and process design method (König et al., 2020b) to the remaining 47 renewable fuel species and their selective production routes with additional consideration of blending fossil gasoline. For each engine type, we derive fuel requirements based on the existing European fuel standards (DIN Deutsches Institut fuer Normung e.V., 2017, 2018) and previously published fuel requirements of UHEEs (Dahmen & Marquardt, 2017; König et al., 2020b).

The resulting optimized fuels and associated production routes confirm fossil gasoline to be the least expensive fuel whereas for minimal GWI, fully renewable fuels have been designed, which come at high costs. For UHEEs and FFVEs, however, strong GWI reductions can be achieved at only slightly higher costs compared to fossil gasoline. In particular, we designed a fully renewable optimal UHEE fuel, which shows a GWI reduction of 70% compared to gasoline and cost increases that lie within ranges that could be compensated by tax reductions on renewable fuels. This favorable performance is achieved by a highly-integrated bio-based production process. Similar fuel production performances are achieved with optimized FFVE fuels that contain small amounts of conventional gasoline. These promising results demonstrate model-based integrated fuel and process design as a powerful method capable of optimizing fuels and their production in a unique way that accounts for the interdependence between feasible fuel compositions and efficient (co-)production.

The comparison of selectively-produced optimized fuels for different ICE types shows that FFVE and UHEE fuels outperform CSIE fuels with respect to their production cost at a specific GWI reduction. This is due to the fact that the fuel requirements of FFVEs and UHEEs are well-suited to the properties of low-cost, low-GWI oxygenated renewable species whereas for CSIEs, the use of such oxygenates is strongly limited by the strict upper bound on the fuel's oxygen content. The results thus provide one argument for replacing CSIE by FFVE and/or UHEE technology.

7. Acknowledgement

This work has been funded by the Deutsche Forschungsgemeinschaft (DFG, German Research Foundation) under Germany's Excellence Strategy - Cluster of Excellence 2186 "The Fuel Science Center". MD received funding from the Helmholtz Association of German Research Centers. The authors kindly thank Sophia Rupprecht and Yang Wang for their help in researching conversion pathways as well as Dominik Bongartz and Sebastian Heger for their valuable recommendations on overcoming numerical difficulties and categorizing toxicity endpoints, respectively.

8. Author Contribution

AK, JV, MD, and AM formulated the research gap and scope of the study. AK and MS conducted the pre-screening with conceptual input from JV and MD. AK compiled the input data from literature and databases, AK and MS implemented a COSMO-RS-MATLAB interface for automated generation of NRTL parameters. AK and MS calculated the energy requirements of each pathway. AMS and JGR provided pure-component RON and MON predictions for components with unknown experimental RONs and MONs. AK, MS, and MD derived the fuel requirements. AK conducted the optimization, and evaluated the results. AK wrote the original draft. All authors reviewed and edited the manuscript and gave their comments for improvements.

9. Appendix A. Supplementary Material

The following are the Supplementary data to this article: ...

AIChE, 2018. DIPPR 801 Database version 12.3.0. http://www.aiche.org/dippr (accessed: 2020-04-21).

American Chemical Society, 2020. SciFinder - The choice for chemistry research. http://www.cas.org/products/scifinder (accessed: 2020-04-01).

Andersen, V. F., Anderson, J. E., Wallington, T. J., Mueller, S. A., & Nielsen, O. J., 2010. Distillation Curves for Alcohol−Gasoline Blends. Energy Fuels, 24, 2683–2691.

Ariffin Kashinath, S. A., Abdul Manan, Z., Hashim, H., & Wan Alwi, S. R., 2012. Design of green diesel from biofuels using computer aided technique. Comput. Chem. Eng., 41, 88–92.

Aspen Technology, I., 2015. Aspen Plus V.8.8. www.aspentech.com (accessed: 2020-04-26).

ASTM D4814, 2020. Standard Specification for Automotive Spark-Ignition Engine Fuel.

Bao, B., Ng, D. K., Tay, D. H., Jiménez-Gutiérrez, A., & El-Halwagi, M., 2011. A shortcut method for the preliminary synthesis of process-technology pathways: An optimization approach and application for the conceptual design of integrated biorefineries. Comput. Chem. Eng., 35, 1374–1383.

Bausa, J., Watzdorf, R. v., & Marquardt, W., 1998. Shortcut methods for nonideal multicomponent distillation: I. Simple columns. AIChE J., 44, 2181–2198.

Bertran, M.-O., Frauzem, R., Sanchez-Arcilla, A.-S., Zhang, L., Woodley, J. M., & Gani, R., 2017. A generic methodology for processing route synthesis and design based on superstructure optimization. Comput. Chem. Eng., 106, 892–910.

Biegler, L. T., Grossmann, I. E., & Westerberg, A. W., 1997. Systematic methods of chemical process design. Prentice-Hall international series in the physical and chemical engineering sciences. Upper Saddle River, NJ: Prentice-Hall.

Boot, M. (Ed.), 2016. Biofuels from lignocellulosic biomass: Innovations beyond bioethanol. Weinheim: Wiley-VCH.

Boot, M. D., Tian, M., Hensen, E. J., & Mani Sarathy, S., 2017. Impact of fuel molecular structure on auto-ignition behavior – Design rules for future high performance gasolines. Prog. Energy Combust. Sci., 60, 1–25.

Chupka, G. M., Christensen, E., Fouts, L., Alleman, T. L., Ratcliff, M. A., & McCormick, R. L., 2015. Heat of vaporization measurements for ethanol blends up to 50 volume percent in several hydrocarbon blendstocks and implications for knock in SI engines. SAE Int. J. Fuels Lubr., 8, 251–263.

Conte, E., Gani, R., & Malik, T. I., 2011. The virtual Product-Process Design laboratory to manage the complexity in the verification of formulated products. Fluid Phase Equilib., 302, 294–304.

Couhert, C., Commandre, J.-M., & Salvador, S., 2009. Is it possible to predict gas yields of any biomass after rapid pyrolysis at high temperature from its composition in cellulose, hemicellulose and lignin? Fuel, 88, 408–417.

Dahmen, M., & Marquardt, W., 2016. Model-Based Design of Tailor-Made Biofuels. Energy Fuels, 30, 1109–1134.

Dahmen, M., & Marquardt, W., 2017. Model-Based Formulation of Biofuel Blends by Simultaneous Product and Pathway Design. Energy Fuels, 31, 4096–4121.

Derfer, J. M., Boord, C. E., Burk, F. C., Hess, R. E., Lovell, W. G., Randall, R. A., & Sabina, J. R., 1958. Knocking Characteristics of Pure Hydrocarbons. 100 Barr Harbor Drive, PO Box C700, West Conshohocken, PA 19428-2959: ASTM International.

DIN Deutsches Institut fuer Normung e.V., 2017. DIN EN 228 Automotive fuels - Unleaded petrol - Requirements and test methods; German version.

DIN Deutsches Institut fuer Normung e.V., 2018. DIN EN15293 Automotive fuels - Automotive ethanol (E85) fuel - Requirements and test methods; German version.

Douglas, J. M., 1985. A hierarchical decision procedure for process synthesis. AIChE J., 31, 353–362.

Eckert, E., & Vaněk, T., 2003. Simulation of separation columns using substitute mixtures. Int. Conf. Slovak Soc. Chem. Eng., (pp. 26 – 30 May).

Elsevier Information Systems GmbH, 2020. Reaxys (R). https://www.reaxys.com/ (accessed: 2020-04-01).

Energy Information Administration, 2020. Biofuels explained - Use of ethanol. https://www.eia.gov/energyexplained/biofuels/use-of-ethanol-in-depth.php (accessed: 2020-08-03).

European Commission, 2016. Weekly Oil Bulletin. https://ec.europa.eu/energy/data-analysis/weekly-oil-bulletin (accessed: 2020-03-31).

European Parliament and the Council of the European Union, 2018. Directive (EU) 2018/2001 on the promotion of the use of energy from renewable sources. Off. J. Eur. Unio., (pp. 82–209) https://eur-lex.europa.eu/legal-content/EN/TXT/?uri=uriserv:OJ.L_.2018.328.01.0082.01.ENG&toc=OJ:L:2018:328:TOC (accessed: 2020-04-26).

Everhart & Hoover - Power Line Construction, Inc, 2020. Safety Data Sheet Gasoline, Unleaded. https://www.everhartandhoover.com/sites/default/files/2018-05/Generic%20Gasoline.pdf (accessed: 2020-05-13).

Ford Motor Company, 2020. Explore Ford - Advanced Fuels. https://www.ford.com/commercial-trucks/advanced-fuel/ (accessed: 2020-04-28).

Friedler, F., Fan, L. T., & Imreh, B., 1998. Process network synthesis: Problem definition. Networks, 31, 119–124.

GAMS Development Corporation, 2020. GAMS - general algebraic modeling system Version 30.1. www.gams.com (accessed: 2020-09-29).

Garcia, D. J., & You, F., 2015. Multiobjective optimization of product and process networks: General modeling framework, efficient global optimization algorithm, and case studies on bioconversion. AIChE J., 61, 530–554.

Gil, J., Corella, J., Aznar, M. P., & Caballero, M. A., 1999. Biomass gasification in atmospheric and bubbling fluidized bed: Effect of the type of gasifying agent on the product distribution. Biomass Bioenergy, 17, 389–403.

Gmehling, J., Kleiber, M., Kolbe, B., & Rarey, J., 2012. Chemical Thermodynamics for Process Simulation. Weinheim, Germany: Wiley-VCH.

Götz, M., Lefebvre, J., Mörs, F., McDaniel Koch, A., Graf, F., Bajohr, S., Reimert, R., & Kolb, T., 2016. Renewable Power-to-Gas: A technological and economic review. Renew. Energy, 85, 1371–1390.

Grube, T., & Höhlein, B., 2014. Kosten der Wasserstoffbereitstellung in Versorgungssystemen auf Basis erneuerbarer Energien. In J. Töpler, & J. Lehmann (Eds.), Wasserstoff und Brennstoffzelle (pp. 225–239). Berlin, Heidelberg: Springer Berlin Heidelberg.

Gschwend, D., Soltic, P., Wokaun, A., & Vogel, F., 2019. Review and Performance Evaluation of Fifty Alternative Liquid Fuels for Spark-Ignition Engines. Energy Fuels, 33, 2186–2196.

Hada, S., Solvason, C. C., & Eden, M. R., 2014. Characterization-based molecular design of bio-fuel additives using chemometric and property clustering techniques. Front. Energy Res., 2, 20.

Haimes, Y. Y., Lasdon, L. S., & Wismer, D. A., 1971. On a Bicriterion Formulation of the Problems of Integrated System Identification and System Optimization. IEEE Trans. Syst. Man. Cybern., 1, 296–297.

Hall, K. R., 2000. Vapor Pressure and Antoine Constants for Oxygen Containing Organic Compounds volume 20B. Berlin/Heidelberg: Springer-Verlag.

Hashim, H., Narayanasamy, M., Yunus, N. A., Shiun, L. J., Muis, Z. A., & Ho, W. S., 2017. A cleaner and greener fuel: Biofuel blend formulation and emission assessment. J. Clean Prod., 146, 208–217.

Hoppe, F., Heuser, B., Thewes, M., Kremer, F., Pischinger, S., Dahmen, M., Hechinger, M., & Marquardt, W., 2015. Tailor-made fuels for future engine concepts. Int. J. Engine. Res., 17, 16–27.

Huber, G. W., Iborra, S., & Corma, A., 2006. Synthesis of transportation fuels from biomass: chemistry, catalysts, and engineering. Chem. Rev., 106, 4044–4098.

International Institute for Sustainability Analysis and Strategy, 2015. GEMIS Software. `www.iinas.org` (accessed: 2020-04-26).

International Organization for Standardization, 2014a. Petroleum products - Determination of knock characteristics of motor and aviation fuels - Motor method (ISO 5163:2014); German version EN ISO 5163:2014.

International Organization for Standardization, 2014b. Petroleum products - Determination of knock characteristics of motor fuels - Research method (ISO 5164:2014); German version EN ISO 5164:2014.

Jaksland, C. A., Gani, R., & Lien, K. M., 1995. Separation Process Design and Synthesis based on Thermodynamic Insights. Chem. Eng. Sci., 50, 511–530.

Johnson, T., & Joshi, A., 2018. Review of Vehicle Engine Efficiency and Emissions. SAE Int. J. Engines, 11, 1307–1330.

Kalakul, S., Zhang, L., Fang, Z., Choudhury, H. A., Intikhab, S., Elbashir, N., Eden, M. R., & Gani, R., 2018. Computer aided chemical product design – ProCAPD and tailor-made blended products. Comput. Chem. Eng., 116, 37–55.

Karavalakis, G., Short, D., Vu, D., Russell, R., Hajbabaei, M., Asa-Awuku, A., & Durbin, T. D., 2015. Evaluating the Effects of Aromatics Content in Gasoline on Gaseous and Particulate Matter Emissions from SI-PFI and SIDI Vehicles. Environ. Sci. Technol., 49, 7021–7031.

Kasten, P., Blanck, R., Loreck, C., Hacker, F., & Forin, S., 2013. Working Paper - Strombasierte Kraftstoffe im Vergleich – Stand heute und die Langfristperspektive. `www.oeko.de/oekodoc/1826/2013-496-de.pdf` (accessed: 2020-04-26).

Kelloway, A., & Daoutidis, P., 2014. Process Synthesis of Biorefineries: Optimization of Biomass Conversion to Fuels and Chemicals. Ind. Eng. Chem. Res., 53, 5261–5273.

Khajavirad, A., & Sahinidis, N. V., 2018. A hybrid LP/NLP paradigm for global optimization relaxations. Math. Prog. Comp., 10, 383–421.

Kim, K.-J., & Diwekar, U. M., 2002. Integrated Solvent Selection and Recycling for Continuous Processes. Ind. Eng. Chem. Res., 41, 4479–4488.

Klamt, A., 2019. COSMOthermX19. `www.cosmologic.de` (accessed: 2020-04-02).

Knop, V., Loos, M., Pera, C., & Jeuland, N., 2014. A linear-by-mole blending rule for octane numbers of n-heptane/iso-octane/toluene mixtures. Fuel, 115, 666–673.

Kohli, K., Prajapati, R., & Sharma, B., 2019. Bio-Based Chemicals from Renewable Biomass for Integrated Biorefineries. Energies, 12, 233.

König, A., Marquardt, W., Mitsos, A., Viell, J., & Dahmen, M., 2020a. Integrated design of renewable fuels and their production processes: Recent advances and challenges. Curr. Opin. Chem. Eng., 27, 45–50.

König, A., Neidhardt, L., Viell, J., Mitsos, A., & Dahmen, M., 2020b. Integrated Design of Processes and Products: Optimal Renewable Fuels. Comput. Chem. Eng., (p. 106712).

König, A., Ulonska, K., Mitsos, A., & Viell, J., 2019. Optimal Applications and Combinations of Renewable Fuel Production from Biomass and Electricity. Energy Fuels, 33, 1659–1672.

Kraemer, K., Harwardt, A., Skiborowski, M., Mitra, S., & Marquardt, W., 2011. Shortcut-based design of multicomponent heteroazeotropic distillation. Chem. Eng. Res. Des., 89, 1168–1189.

Lange, J.-P., 2001. Fuels and Chemicals Manufacturing; Guidelines for Understanding and Minimizing the Production Costs. Cattech, 5, 82–95.

Lange, J.-P., Price, R., Ayoub, P. M., Louis, J., Petrus, L., Clarke, L., & Gosselink, H., 2010. Valeric biofuels: a platform of cellulosic transportation fuels. Angew. Chem. Int. Ed. Engl., 49, 4479–4483.

Larsen, U., Johansen, T., & Schramm, J., 2009. Ethanol as a fuel for road transportation. `https://amf-tcp.org/app/webroot/files/file/Annex%20Reports/AMF_Annex_35-1.pdf` (accessed: 2020-04-27).

Leitner, W., Klankermayer, J., Pischinger, S., Pitsch, H., & Kohse-Höinghaus, K., 2017. Advanced Biofuels and Beyond: Chemistry Solutions for Propulsion and Production. Angew. Chem. Int. Ed. Engl., 56, 5412–5452.

Manonmani, H. K., & Sreekantiah, K. R., 1987. Saccharification of sugar-cane bagasse with enzymes from Aspergillus ustus and Trichoderma viride. Enzyme Microb. Technol., 9, 484–488.

Markel, A. J., & Bailey, B. K., 1998. Modeling and cold start in alcohol-fueled engines. `https://www.osti.gov/biblio/650264` (accessed: 2020-05-05).

Marquardt, W., Harwardt, A., Hechinger, M., Kraemer, K., Viell, J., & Voll, A., 2010. The biorenewables opportunity - toward next generation process and product systems. AIChE J., 56, 2228–2235.

Marvin, W. A., Rangarajan, S., & Daoutidis, P., 2013. Automated Generation and Optimal Selection of Biofuel-Gasoline Blends and Their Synthesis Routes. Energy Fuels, 27, 3585–3594.

McCormick, R. L., Fioroni, G., Fouts, L., Christensen, E., Yanowitz, J., Polikarpov, E., Albrecht, K., Gaspar, D. J., Gladden, J., & George, A., 2017. Selection Criteria and Screening of Potential Biomass-Derived Streams as Fuel Blendstocks for Advanced Spark-Ignition Engines. SAE Int. J. Fuels Lubr., 10, 442–460.

Naegeli, D. W., Yost, D. M., Moulton, D. S., Owens, E. C., & Chui, G. K., 1989. The Measurement of Octane Numbers for Methanol and Reference Fuels Blends. SAE Trans. Int. J. Fuels Lubr., 98, 712–722.

Papadopoulos, A. I., & Linke, P., 2006. Efficient integration of optimal solvent and process design using molecular clustering. Chem. Eng. Sci., 61, 6316–6336.

Perez, P. L., & Boehman, A. L., 2012. Experimental Investigation of the Autoignition Behavior of Surrogate Gasoline Fuels in a Constant-Volume Combustion Bomb Apparatus and Its Relevance to HCCI Combustion. Energy Fuels, 26, 6106–6117.

Prakash, A., Redmann, J.-H., Giles, K., Cracknell, R., Turner, N., Aradi, A. A., Lewis, A., & Akehurst, S., 2018. Octane Response of a Highly Boosted Direct Injection Spark Ignition Engine at Different Compression Ratios. SAE Tech. Pap., (pp. 1–11).

Quader, M. A., Ahmed, S., Raja Ghazilla, R. A., Ahmed, S., & Dahari, M., 2016. Evaluation of criteria for CO2 capture and storage in the iron and steel industry using the 2-tuple DEMATEL technique. J. Clean Prod., 120, 207–220.

Rangarajan, S., Bhan, A., & Daoutidis, P., 2010. Rule-Based Generation of Thermochemical Routes to Biomass Conversion. Ind. Eng. Chem. Res., 49, 10459–10470.

Rangarajan, S., Bhan, A., & Daoutidis, P., 2012. Language-oriented rule-based reaction network generation and analysis: Description of RING. Comput. Chem. Eng., 45, 114–123.

Rangarajan, S., Kaminski, T., van Wyk, E., Bhan, A., & Daoutidis, P., 2014. Language-oriented rule-based reaction network generation and analysis: Algorithms of RING. Comput. Chem. Eng., 64, 124–137.

Reiter, A. M., Wallek, T., Pfennig, A., & Zeymer, M., 2015. Surrogate generation and evaluation for diesel fuel. Energy Fuels, 29, 4181–4192.

Remmert, S. M., Cracknell, R. F., Head, R., Schuetze, A., Lewis, A., Akehurst, S., Turner, J., & Popplewell, A., 2014. Octane Response in a Downsized, Highly Boosted Direct Injection Spark Ignition Engine. SAE Int. J. Fuels Lubr., 7, 131–143.

Renon, H., & Prausnitz, J. M., 1968. Local compositions in thermodynamic excess functions for liquid mixtures. AIChE J., 14, 135–144.

Ruth, M., 2011. Hydrogen Production Cost Estimate Using Biomass Gasification: Independent Review: Technical Report DE-AC36-08GO28308 National Renewable Energy Laboratory. https://www.hydrogen.energy.gov/pdfs/51726.pdf (accessed: 2020-04-01).

Sarathy, S. M., Kukkadapu, G., Mehl, M., Javed, T., Ahmed, A., Naser, N., Tekawade, A., Kosiba, G., AlAbbad, M., Singh, E., Park, S., Rashidi, M. A., Chung, S. H., Roberts, W. L., Oehlschlaeger, M. A., Sung, C.-J., & Farooq, A., 2016. Compositional effects on the ignition of FACE gasolines. Combust. Flame, 169, 171–193.

Schack, D., Liesche, G., & Sundmacher, K., 2020. The FluxMax approach: Simultaneous flux optimization and heat integration by discretization of thermodynamic state space illustrated on methanol synthesis process. Chem. Eng. Sci., 215, 115382.

SCHC-OSHA Alliance GHS/HazCom Information Sheet Workgroup, 2017. Hazard Communication Information Sheet Reflecting the US OSHA Implementation of the Globally Harmonized System (GHS) of Classification and Labelling of Chemicals: Acute Toxixity - Inhalation. https://www.schc.org/assets/

docs/ghs_info_sheets/acute_toxicity_inhalation_2017_07.pdf (accessed: 2020-04-02).

Scheffczyk, J., Schäfer, P., Fleitmann, L., Thien, J., Redepenning, C., Leonhard, K., Marquardt, W., & Bardow, A., 2018. COSMO-CAMPD: A framework for integrated design of molecules and processes based on COSMO-RS. Mol. Syst. Des. Eng., 3, 645–657.

Schweidtmann, A. M., Rittig, J. R., König, A., Dahmen, M., Grohe, M., & Mitsos, A., 2020. Graph Neural Networks for Prediction of Fuel Ignition Quality. https://gnn.avt.rwth-aachen.de/ (accessed: 2020-06-16). doi:10.26434/chemrxiv.12280325.v1.

Sjöberg, M., 2017. An Introduction to DOE's Co-Optima Initiative. https://www.osti.gov/servlets/purl/1466483 (accessed: 2020-04-27).

Steimel, J., Harrmann, M., Schembecker, G., & Engell, S., 2014. A framework for the modeling and optimization of process superstructures under uncertainty. Chem. Eng. Sci., 115, 225–237.

Straathof, A. J. J., 2014. Transformation of Biomass into Commodity Chemicals Using Enzymes or Cells. Chem. Rev., 114, 1871–1908.

Teter, J., Le Feuvre, P., Gorner, M., & Scheffer, S., 2019. Tracking Transport. https://www.iea.org/reports/tracking-transport-2019 (accessed: 2020-04-02).

Tremel, A., Wasserscheid, P., Baldauf, M., & Hammer, T., 2015. Techno-economic analysis for the synthesis of liquid and gaseous fuels based on hydrogen production via electrolysis. Int. J. Hydrogen Energy, 40, 11457–11464.

Tsagkari, M., Couturier, J.-L., Kokossis, A., & Dubois, J.-L., 2016. Early-Stage Capital Cost Estimation of Biorefinery Processes: A Comparative Study of Heuristic Techniques. ChemSusChem, 9, 2284–2297.

Ulonska, K., Skiborowski, M., Mitsos, A., & Viell, J., 2016a. Early-stage evaluation of biorefinery processing pathways using process network flux analysis. AIChE J., 62, 3096–3108.

Ulonska, K., Voll, A., & Marquardt, W., 2016b. Screening Pathways for the Production of Next Generation Biofuels. Energy Fuels, 30, 445–456.

Villeda, J. V., Dahmen, M., Hechinger, M., Voll, A., & Marquardt, W., 2012. Towards model-based design of biofuel value chains. Curr. Opin. Chem. Eng., 1, 465–471.

Voll, A., & Marquardt, W., 2012. Reaction network flux analysis: Optimization-based evaluation of reaction pathways for biorenewables processing. AIChE J., 58, 1788–1801.

Wei, J., Yin, Z., Qian, Y., Wang, C., & Chen, B., 2019. Comparative Effects of Olefin Content on the Performance and Emissions of a Modern GDI Engine. Energy Fuels, 33, 10499–10507.

Yanowitz, J., Christensen, E., & McCormick, R. L., 2011. Utilization of Renewable Oxygenates as Gasoline Blend Components: Technical Report NREL/TP-5400-50791 National Renewable Energy Laboratory. http://www.nrel.gov/docs/fy11osti/50791.pdf (accessed: 2020-03-31).

Yaws, C. L., & Satyro, M. A., 2015. Vapor Pressure – Organic Compounds. In The Yaws Handbook of Vapor Pressure (pp. 1–314). Elsevier.

Yunus, N. A., Gernaey, K. V., Woodley, J. M., & Gani, R., 2014. A systematic methodology for design of tailor-made blended products. Comput. Chem. Eng., 66, 201–213.

Zhang, L., Kalakul, S., Liu, L., Elbashir, N. O., Du, J., & Gani, R., 2018. A Computer-Aided Methodology for Mixture-Blend Design. Applications to Tailor-Made Design of Surrogate Fuels. Ind. Eng. Chem. Res., 57, 7008–7020.

Zhou, T., Zhou, Y., & Sundmacher, K., 2017. A hybrid stochastic–deterministic optimization approach for integrated solvent and process design. Chem. Eng. Sci., 159, 207–216.